Global and Planetary Change 232 (2024) 104321

Contents lists available at ScienceDirect

Global and Planetary Change

journal homepage: www.elsevier.com/locate/gloplacha

Constraining the end of the Last Interglacial (MIS 5e) relative sea-level highstand in central Mediterranean: New data from Grotta delle Capre, central Italy

Biagio Giaccio [a,*], Monica Bini [b,c,d], Ilaria Isola [d], Hsun-Ming Hu [e], Mario Federico Rolfo [g], Shen Chuan-Chou [e,f], Angelica Ferracci [g], Lorenzo Monaco [b], Francesca Pasquetti [b], Giovanni Zanchetta [b,c,d]

[a] Institute of Environmental Geology and Geoengineering, IGAG-CNR, 00015 Montelibretti, Rome, Italy
[b] Department of Earth Sciences, University of Pisa, Pisa, Italy
[c] Centre for Climatic Change Impact, CIRSEC, University of Pisa, Pisa, Italy
[d] Istituto Nazionale di Geofisica e Vulcanologia, Pisa, Italy
[e] High-Precision Mass Spectrometry and Environment Change Laboratory (HISPEC), Department of Geosciences, National Taiwan University, Taipei 10617, Taiwan, ROC.
[f] Research Center for Future Earth, National Taiwan University, Taipei 10617, Taiwan, ROC.
[g] Department of History, Culture and Society, University of Rome "Tor Vergata", Rome, Italy

ARTICLE INFO

Editor Name: Dr. Fabienne Marret-Davies

Keywords:
Last Interglacial
Relative sea-level
U/Th chronology
Terrestrial limiting points
Mediterranean

ABSTRACT

The current rapid change of the Earth's climate has resulted in an increasing interest for the past warm periods as potential long-term scenarios of the effects of the present global warming. The last such a period occurred 129–116 ka, known as the Last Interglacial (LIG), when the continental ice volume was significantly smaller than present, leading to a global sea-level (GSL) higher than present one. Detailed morpho-stratigraphic data, supported by a robust U/Th chronology, from Grotta delle Capre, central Italy, provided new chronological insights on the relative sea-level (RSL) dynamic during the LIG in the Mediterranean region. Our results indicate that, on Tyrrhenian Sea coasts of the central Italy, after having stationed at ~9 m a.s.l., the LIG RSL fell at an elevation <3 m a.s.l. as early as before 123 ka, and then no longer rose above this elevation either during the later stages of the LIG or afterwards. The results match previous studies based on U/Th dating of terrestrial limiting points from Grotta Infreschi, ~200 km SE from Grotta delle Capre along the same Tyrrhenian Sea coasts, and are in agreement with the Red Sea RLS and GSL records and the probabilistic LIG sea level assessments based on globally distributed records. On the other hand, our reconstruction is not supported by implications of U/Th dating of corals and phreatic overgrowth on speleothems from the Balearic Island of Mallorca. Such an inconsistency in the overall knowledge around the LIG RSL reconstruction results in a high uncertainty in modelling the ice and sea-level dynamic during this warm period, which needs to be reduced through more and more high-resolution, stratigraphic and chronological investigations of the morphological and sedimentary sea-level records.

1. Introduction

The Last Interglacial (LIG, ~129–116 ka, e.g., Stirling et al., 1998; Muhs, 2002; Muhs et al., 2015), roughly matching the Marine Isotope Stage (MIS) 5e (Govin et al., 2015; Rovere et al., 2015; Dutton et al., 2015), is considered a potentially useful analogue to study Earth climate in a condition of excess of warmth (e.g., Otto-Bliesner et al., 2006; Clark and Huybers, 2009; Hoffman et al., 2017), though the boundary conditions were quite different from the current anthropogenic-driven global warming. Specifically, a stronger summer insolation and a CO_2 concentration higher than pre-industrial Holocene, may have promoted a peak of the global mean temperature ~ 0.8 °C above pre-industrial values (CAPE-LIG Project Members, 2016; PIGS Working Group of PAGES, 2016; Lüthi et al., 2008; Hoffman et al., 2017). In turn, this

* Corresponding author.
E-mail address: biagio.giaccio@cnr.it (B. Giaccio).

https://doi.org/10.1016/j.gloplacha.2023.104321
Received 13 June 2023; Received in revised form 3 November 2023; Accepted 21 November 2023
Available online 25 November 2023

resulted in a reduction of the continental ice volume and a consequent rising of the global mean sea-level (GMSL), whose estimates are still matter of debate (e.g., Rohling et al., 2009; Kopp et al., 2009; O'Leary et al., 2013; Dutton et al., 2015; Dyer et al., 2021). The study of the LIG sea-level is, therefore, considered of particular relevance for investigating the response of the cryosphere to a warmer world and can give useful insights for future scenarios linked to global warming (e.g., Alley et al., 2005; Rohling et al., 2009; Kopp et al., 2009; Joughin and Alley, 2011; Levermann et al., 2013; Burke et al., 2018; Capron et al., 2019), especially for the very high scenarios of CO_2 emission (IPCC, 2023). However, reconstructing the detailed timing and dynamic of the sea-level oscillations during the LIG is still a challenge. Some studies recognized that there have been more than one oscillation (Hearty et al., 2007; Kopp et al., 2009; Thompson et al., 2011; Medina-Elizalde, 2013; Rohling et al., 2019), while others support the notion of a relative sea level-stability (e.g., Barlow et al., 2018; Polyak et al., 2018). Constraining radiometrically the LIG sea-level dynamic can be a hard task and different approaches have been used to assess it (Rohling et al., 2009; Kopp et al., 2009; O'Leary et al., 2013). However, high-quality radiometric dating remains pivotal to reliably constraining the temporal and spatial evolution of the LIG relative sea-level (RSL) (e.g., Dutton et al., 2015; Hibbert et al., 2016; Pasquetti et al., 2021; Rovere et al., 2023).

The Mediterranean coasts preserve abundant evidence of the LIG sea level highstand (e.g., Hearty et al., 1986; Hillaire-Marcel et al., 1996; Antonioli et al., 2015) in the form of marine terraces, beach deposits and erosive features (e.g. notches, shore platforms), which have extensively been revised in recent papers (e.g., Antonioli et al., 2018; Cerrone et al., 2021; Dumitru et al., 2021; Pasquetti et al., 2021; Marra et al., 2019, 2020, 2023). Despite the application of different dating methods (e.g., U/Th: Hillaire-Marcel et al., 1996; Amino Acid racemization: Hearty et al., 1986; Optical Stimulated Luminescence -OSL- Mauz, 1999), the current chronological accuracy has made it challenging to attribute geomorphological forms and/or deposits to the LIG (Pasquetti et al., 2021; Cerrone et al., 2021 and references therein). A suite of U/Th dating on corals and speleothems overgrowths at Mallorca Island indicates that the LIG RSL highstand was relatively stable and lasted from ~126 to ~118 ka (Muhs et al., 2015; Polyak et al., 2018). More recently Bini et al. (2020), dating a suite of phreatic speleothems as terrestrial limiting points (i.e., the speleothems that lie above the High Astronomical Tide -HAT-, thus the RSL was lower than the position of the speleothem deposition, e.g., Rovere et al., 2016) in the archeological cave of Infreschi (southern Italy), found a substantial drop in the RSL of several meters already before 120 ka. These regional differences can be accounted by different glacial isostatic adjustment (GIA) background (e.g., Stocchi et al., 2018), and/or tectonic components. However, the possibility to test GIA models and/or estimate tectonic components for the region is largely hindered by the necessity to produce a better chronological framework of the LIG highstand successions in the Mediterranean (Pasquetti et al., 2021).

With the aim of improving the knowledge on the dynamics of the LIG highstand, we investigated the sedimentary infilling and the

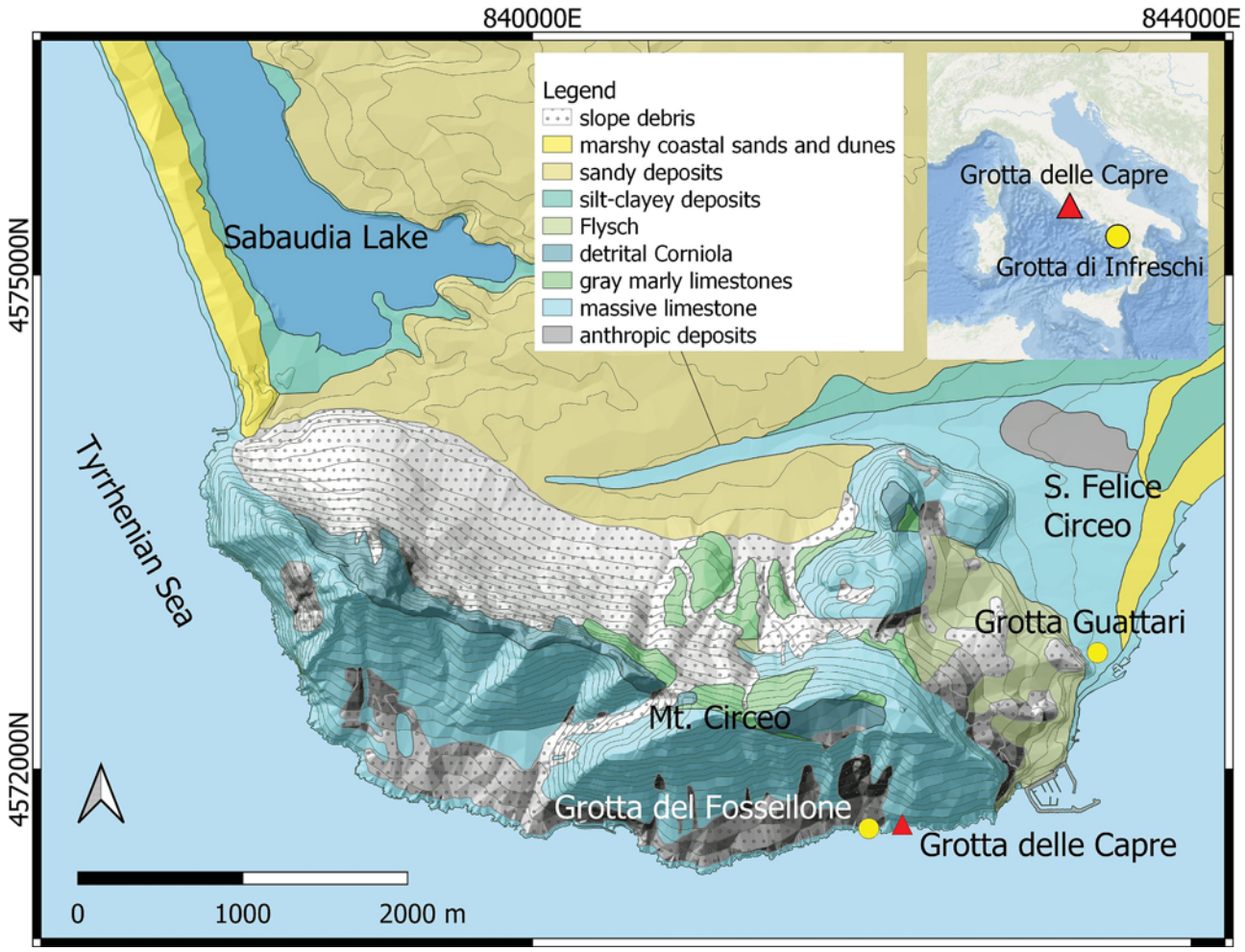

Fig. 1. Simplified geological map of Mt. Circeo (https://geoportale.regione.lazio.it/geoserver) with location of Grotta delle Capre. Inset, reference map of the Grotta delle Capre and of previously investigated Infreschi Cave (Bini et al., 2020).

geomorphological features of Grotta delle Capre (literally "Goat Cave"), a coastal cave along the central Italy Tyrrhenian side (Fig. 1). The study was supported by a new suite of U/Th dating of terrestrial limiting points that provided new insights on the timing of the sea level drop following the LIG highstand.

2. Site description and previous investigations

Grotta delle Capre opens on the southern slope of Monte Circeo in the Mesozoic carbonate units (Segre, 1991) (Fig. 1). It belongs to a system of marine caves along the coast containing continental infilling renowned for their Middle to Upper Paleolithic archeological remains (e.g., Blanc and Segre, 1953; Bietti and Grimaldi, 1991).

The first modern report on the stratigraphy of the cave is due to Blanc and Segre (1953), who performed a detailed reconstruction of the stratigraphy at the entrance of the cave and described the presence of *Lithophaga (date mussels or boring mussels)* boreholes band up to nine m a.s.l., which was also previously observed by Issel (1883). Blanc and Segre (1953) recognized 12 layers. The lowest layer (layer 1 for Blanc and Segre, 1953), resting on the carbonate bedrock, was described as a marine coastal deposit containing marine mollusks and related to the "Tyrrhenian" (often synonymous today with the LIG highstand). Durante and Settepassi (1974) reported a new description of the stratigraphy of the cave which is close to that proposed by Blanc and Segre (1953), but consisting of 9 main layers. They recognized two sea-level highstand markers: the upper one marked by a marine notch accompanied by the upper level of *Lithophaga* boreholes at ~8 m a.s.l, and the lower one corresponding to the basal beach deposit (layer 9 for Durante and Settepassi, 1974, corresponding to the layer 1 of Blanc and Segre, 1953). These two marine phases were related to the Eutyrrhenian (the upper limit of *Lithophaga* boreholes band) and the Neotyrrhenian (the beach deposits) following the popular scheme proposed for the Mediterranean area by Bonifay and Mars (1959). Durante and Settepassi (1974) performed a detailed description of the marine faunas contained in the basal marine deposit (layer 9) reporting at least three species characteristic of the warm water fauna typical of the "Tyrrhenian": *Cymatium ficoides*, *Bursa (Crustata) pustulosa*, and *Lithodomus (Myoforcepts) caudigerus*.

Ruffo and Zarattini (1991) performed an archeological excavation and reported additional stratigraphic data. They again described the upper limit of sub-horizontally boreholes of *Lithophaga lithophaga* between ~8–10 m a.s.l. The general stratigraphy, though more detailed resulting from observation during the archeological excavation, is comparable with those proposed by Blanc and Segre (1953) and Durante and Settepassi (1974). However, they noted for the first time the enrichment in volcanic elements (i.e., pumices and glass shards) in some layers, and reported the presence of discontinuous "stalagmitic" formation directly above the coastal marine deposits. Antonioli et al. (2018) described in detail the upper sea-level highstand marker (i.e. the marine notch), reporting an altitude of 9.28 ± 0.18 m a.s.l. and attributing this sea-level marker to the LIG highstand based on the finding of the warm species *Thetystrombus latus* (previously named *Strombus bubonius*; e.g., Taviani, 2014), which is characteristic of the Mediterranean LIG highstand deposits, in the near succession of the Grotta del Fossellone (Durante, 1975). More recently, Marra et al. (2023) performed new stratigraphic and geochronological investigations on the cave succession. They recognized the notch described in previous studies providing a new measurement of its elevation at 9.5 ± 0.2 m a.s.l. and subdivided the sedimentary succession into five main stratigraphic units, from the younger SU1 to the older SU5. Marra et al. (2003) also provided the first radioisotopic dating for the sedimentary succession based on $^{40}Ar/^{39}Ar$ dating of primary and sub-primary tephra layers, supporting the attribution of the tidal notch and of the beach deposits to the LIG. In conclusion, all the previous studies are consistent in describing (i) the presence of a higher sea-level marker characterized by a sub horizontal level of *Lithophaga* boreholes and a notch at about the same height, (ii) a "basal" coarse beach deposit, and (iii) a continental succession laying on the beach sediments, as summarized in Fig. 2.

3. Materials and methods

3.1. Field and topographic investigations

A new survey was conducted between 2020 and 2022, producing a new lithostratigraphic description followed by the collection of several samples for U/Th dating (carbonate concretions and speleothems) and tephrochronological analyses (glass-composition).

The direct measurement with DGPS of the RSL indicators (i.e., notch and *Lithophaga* burrows) or terrestrial limiting points (i.e., speleothems, tephra layers) along the sedimentary succession was not possible because of their position inside the cave. To overcome this problem we used the Trimble®R10 GNSS (Global Navigation Satellite System) to measure the elevation of a point located in front of the cave entrance (Table TS1) and then we reported the measurements of all indicators at this point using graduated rods equipped with a spirit level. This selected point marked the limit of the local biological mean sea-level indicators (Vacchi et al., 2020), which in microtidal Mediterranean settings correspond the mean sea-level with reasonable accuracy (±0.1 m, e.g. Vacchi et al., 2020 and reference therein). The Trimble®R10 GNSS was employed with RTK Quick-point acquisition method. Subsequently, we performed post-processing and referenced the measurement to the current geoid model ITALGEO2005. Taking into account the vertical precision, the finest R10's measure introduced an error of ±0.035 m, post-processing introduced an error of ±0.066 m, and the use of spirit bars introduced an error of ±0.1 m (Bini et al., 2018; Zanchetta et al., 2014). Therefore, we can approximate the overall vertical error to ±0.15 m as calculated using methods described in Shennan et al. (2015) (Table S1 and S2).

3.2. U/Th geochronology

Speleothem samples GDC5 and GDC9 for U/Th dating were collected along the exposed section at the cave entrance (Figs. 2 and 3) to chronologically constrain the sediment infill succession. Two additional flowstone samples, covering the notch and the *Lithophaga* boreholes (GDC12, Fig. 2c) and the beach deposits in the innermost part of the cave (GDC3, Fig. 2c), were collected to get a *terminus ante quem* (i.e., a chronological indication before of which these sediments formed) for these sea-level markers.

The samples were cut and polished at the Laboratory of Paleoclimatology and Geoarchaeology of the University of Pisa. The U/Th dating on the chipped subsamples was performed at the High-Precision Mass Spectrometry and Environment Change Laboratory (HISPEC), Department of Geosciences, National Taiwan University. All U–Th chemistry and isotopic measurements were conducted on a Thermo-Finnigan Neptune multi-collector inductively coupled plasma mass spectrometer (Shen et al., 2008, 2012; Cheng et al., 2013). A gravimetrically calibrated triple-spike, ^{229}Th-^{233}U-^{236}U, and the isotope dilution method (Shen et al., 2003) were employed to correct for mass bias and to determine U–Th isotopic compositions and contents (Shen et al., 2003). Half-lives of U–Th nuclides used for ^{230}Th age calculation are given in Cheng et al. (2013). Uncertainties in isotopic data and ^{230}Th dates are given at the two-sigma (2σ) level or two standard deviations of the mean ($2\sigma_m$) unless otherwise noted. An initial $^{230}Th/^{232}Th$ atomic ratio of $(4 \pm 2) \times 10^{-6}$ was applied for age correction. Results are shown in Table 1.

3.3. Tephrochronology

3.3.1. Glass chemical composition

The tephra or volcaniclastic layers LU4, LU6 and LU 9 (Fig. 3) were

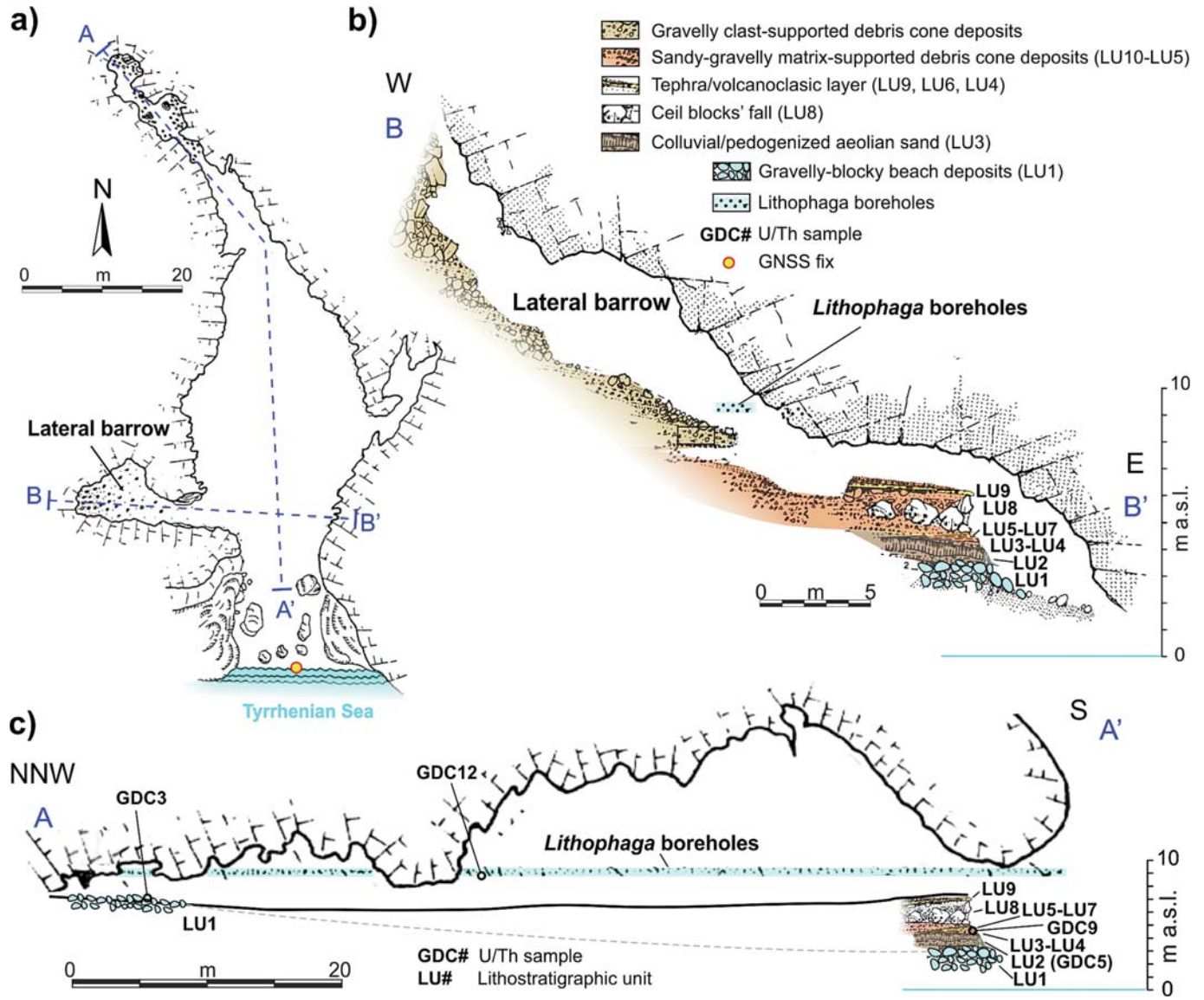

Fig. 2. Planimetry (a) and cross topographic/stratigraphic sections (b–c) of Grotta delle Capre (modified from Ruffo and Zarattini 1991).

sampled for glass geochemical fingerprinting, aimed at correlating them with possible well-dated proximal or distal equivalents. The samples were wet-sieved, observed under binocular microscope and then mounted on polished slides for major element glass composition analyses, using a Cameca SX50 electron microprobe, equipped with a five-wavelength dispersive spectrometer, at Istituto di Geologia Ambientale e Geoingegneria of the Italian National Research Council (IGAG-CNR) of Montelibretti, Rome. Operating conditions and internal and external standards were the same as described in Monaco et al. (2022).

4. Results

4.1. Morpho-stratigraphy

The cave opens seaward to the south, through a wide entrance on a steep cliff and presents an elongated planimetry (~60 m long and ~20 m wide) that becomes narrower in the innermost part (Fig. 2a). The cave connects with the external side also through a minor lateral barrow, which opens along the western wall (Fig. 2a–b). The floor is at an elevation of ~7.5–7.0 m a.s.l and is relatively flat throughout the cave. It subtends the top of the sedimentary infilling, which is exposed close to the main entrance as a cliff due to the active erosion of winter sea storms (Fig. 2c).

The cave walls show a continuous and evident small indentation, the tidal notch described in detail by Antonioli et al. (2018), with the retreat point measured in this work at 9.51 ± 0.14 m a.s.l. Abundant *Lithophaga* boreholes with a clear sub-horizontal limit a few cm above the upper limit of the notch m a.s.l. (Fig. 2b–c) is also present. The sedimentary succession cropping out at the main entrance was subdivided in eleven lithostratigraphic units (LU#), from the lower LU1 to the uppermost LU11 (Figs. 2 and 3), which belong to five main depositional-environmental systems, i.e.; (i) beach deposits, (ii) speleothems, (iii) colluvial deposits, (iv) block fall deposits and (v) alluvial deposits, which can contain sub-primary and reworked volcanic ash layers and stalagmites (Fig. 3).

Beach deposit: (LU1) rests directly on the cave floor and consists of rounded boulders and gravels marked by *Lithophaga* boreholes, with a yellowish sandy and sandy gravels matrix and rare marine fossils (Fig. 3). In the innermost part of the cave, well-rounded pebbles and well-sorted sands, possibly corresponding to LU1, emerge under the terrestrial sediments that likely here become thinner (Fig. 2c). Laterally on the cave wall, LU1 seems to rest on a poorly expressed erosive notch,

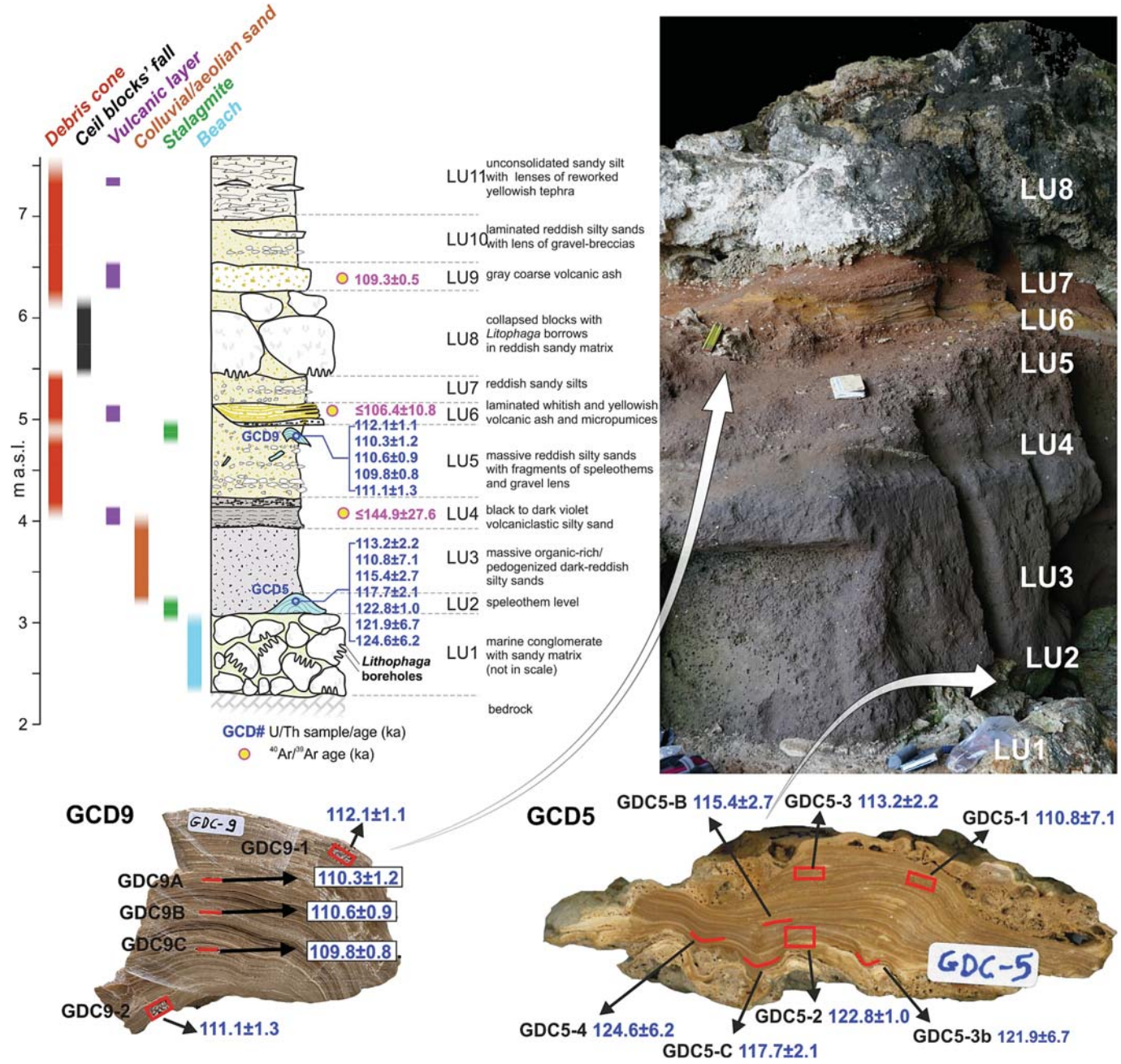

Fig. 3. Stratigraphy and chronology, with detailed location of the U/Th-dated stalagmite sub-samples, of the Grotta delle Capre sedimentary infilling outcropping at cave entrance (Fig. 2). The $^{40}Ar/^{39}Ar$ age of the sub-primary tephra LU9 and volcaniclastic layers LU4 and LU6 are from Marra et al. (2023).

which may correspond to the notch reported by Durante and Settepassi (1974).

Stalagmite (LU2) is a discontinuous thinly laminated speleothem which rests directly on the boulders of the LU1 (Fig. 3). This carbonate concretion (sample GDC-5) displays a basal tufa layer followed by a columnar fabric frequently interrupted by thin (submillimetric) tufa layers (Frisia et al., 2000), ending with a few millimeter thick tufa layer (Fig. S1).

Colluvial deposit (LU3) consists of massive pedogenised dark reddish silty sands. It corresponds to layer 2a of Blanc and Segre, 1953, and part of layer 8 of Durante and Settepassi, 1974 (Fig. 3).

Alluvial deposit (LU4-LU7 and LU9-LU11) consists of a fining upward succession of sand, silt and gravel deposits, representing the lateral etheropic lithofacies of the debris cone developed from the lateral barrow of the cave (Fig. 2). LU4 is a black to dark violet volcaniclastic silty sand composed by garish, poorly vesicular scoria in garish dense microlithic texture of the juvenile clasts (Fig. 3). LU4 correspond to part of layer 2a of Blanc and Segre (1953) and to the sample GDC-6 of Marra et al. (2023), dated to $\leq 144.9 \pm 27.6$ ka. LU5 is a massive reddish sandy-silty deposit with sparse gravel and some evidence of calcite deposition by dripping water and fragmented speleothems dropped from the cave ceiling (i.e., stalactites and soda straws). The deposit also contains remains of bones and land snails shells like *Pomatia elegans*. In particular, at ca. 4 m a.s.l. there is a stalagmite in growth position (Fig. 3). The stalagmite (Sample GDC-9) shows submillimetric lamination with microcrystalline fabric in the basal part followed by columnar elongated fabric on the top (Fig. S1). LU6 is a lenticular layer of well stratified whitish and yellowish fine to medium volcanic ash made of strongly altered whitish-yellowish and moderately vesicular micropumices including secondary blackish manganese nodules. It corresponds to

Table 1
Uranium and thorium isotopic compositions and ^{230}Th ages by MC-ICPMS, Thermo Electron Neptune, at NTU.

Stalagmite	Sample	Weight	^{238}U		^{232}Th		$d^{234}U$		$[^{230}Th/^{238}U]$		$^{230}Th/^{232}Th$		Age (kyr ago)		Age (ka)		$d^{234}U_{initial}$	
		g	10^{-9} g/g[a]		10^{-9} g/g		Measured[a]		Activity[c]		Atomic ($\times 10^{-6}$)		Uncorrected		Corrected[c,d]		Corrected[b]	
GDC-9 (4.00)[e,f]	A	0.0523	123.21	± 0.23	5.78	± 0.14	93.2	± 3.9	0.7085	± 0.0027	248.9	± 5.9	111.5	± 1.1	110.3	± 1.2	127.3	± 5.4
	B	0.0579	101.64	± 0.11	1.7414	± 0.0091	86.3	± 1.7	0.7021	± 0.0029	675.6	± 4.4	111.1	± 0.9	110.6	± 0.9	117.9	± 2.4
	C	0.0570	80.13	± 0.10	1.3489	± 0.0086	81.4	± 1.9	0.6954	± 0.0027	681.1	± 5.0	110.3	± 0.8	109.8	± 0.8	111.0	± 2.6
	1	0.0361	123.37	± 0.13	6.607	± 0.067	84.5	± 2.0	0.7092	± 0.0031	218.3	± 2.4	113.4	± 0.9	112.1	± 1.1	116.0	± 2.7
	2	0.0533	137.28	± 0.14	12.92	± 0.10	81.9	± 1.7	0.7073	± 0.0020	124.0	± 1.0	113.4	± 0.7	111.1	± 1.3	112.1	± 2.3
	B	0.0539	122.38	± 0.13	20.95	± 0.13	164.3	± 1.7	0.7908	± 0.0076	76.18	± 0.86	119.2	± 2.0	115.4	± 2.7	227.6	± 2.9
	C	0.0524	106.37	± 0.12	18.57	± 0.41	164.9	± 1.7	0.8003	± 0.0030	75.6	± 1.7	121.6	± 0.9	117.7	± 2.1	230.0	± 2.7
GDC-5 (3.10)[e,f]	1	0.0563	155.10	± 0.26	88.65	± 0.99	155.6	± 2.9	0.8018	± 0.0042	23.13	± 0.28	124.0	± 1.3	110.8	± 7.1	212.7	± 5.7
	2	0.0568	159.17	± 0.22	4.554	± 0.043	172.3	± 2.3	0.8131	± 0.0032	468.6	± 4.7	123.5	± 1.0	122.8	± 1.0	243.8	± 3.4
	3	0.0544	156.72	± 0.22	28.51	± 0.18	149.1	± 2.4	0.7723	± 0.0027	70.00	± 0.49	117.4	± 0.9	113.2	± 2.2	205.3	± 3.5
	3b	0.0576	161.86	± 0.18	77,168	± 568	160.6	± 1.7	0.836	± 0.013	28.91	± 0.50	132.7	± 3.9	121.9	± 6.7	121.9	± 6.7
	4	0.0548	134.20	± 0.16	69.0	± 2.2	173.8	± 1.7	0.8583	± 0.0037	27.53	± 0.88	136.1	± 1.2	124.6	± 6.2	247.1	± 4.8
GDC-3 (7.40)[e,f]	/	0.0445	78.38	± 0.12	54.89	± 0.39	297.1	± 3.4	0.2136	± 0.0097	5.03	± 0.23	19.5	± 1.0	4.2	± 8.3	300.7	± 7.6
GDC-1 (8.90)[e,f]	2	0.0488	204.5	± 1.1	2.327	± 0.010	356	± 26	0.03190	± 0.00088	46.2	± 1.3	2.6	± 0.1	2.3	± 0.1	358	± 27
	1	0.0618	196.5	± 1.9	2.056	± 0.015	116	± 21	0.0318	± 0.0026	50.1	± 4.1	3.2	± 0.3	2.8	± 0.3	117	± 21

Analytical errors are 2σ of the mean.
Decay constants are 9.1705×10^{-6} yr^{-1} for ^{230Th}, 2.8221×10^{-6} yr^{-1} for ^{234}U (Cheng et al., 2013). and 1.55125×10^{-10} yr^{-1} for ^{238}U (Jaffey et al., 1971).
Those are the values for a material at secular equilibrium, with the crustal $^{232}Th/^{238}U$ value of 3.8. The errors are arbitrarily assumed to be 50%.
[a] $[^{238}U] = [^{235}U] \times 137.818$ (±0.65‰) (Hiess et al., 2012); $d^{234}U = ([^{234}U/^{238}U]_{activity} - 1) \times 1000$.
[b] $d^{234}U_{initial}$ corrected was calculated based on ^{230}Th age (T), i.e., $d^{234}U_{initial} = d^{234}U_{measured} \times e^{l234 \times T}$, and T is corrected age.
[c] $[^{230}Th/^{238}U]_{activity} = 1 - e^{-l230T} + (d^{234}U_{measured}/1000)[l_{230}/(l_{230} - l_{234})](1 - e^{-(l230 - l234) T})$, where T is the age.
[d] Age corrections, relative to 1950 CE, were calculated using an estimated atomic $^{230}Th/^{232}Th$ ratio of 4 (± 2) x 10^{-6}.
[e] Elevation of the sample in m (associated error ± 0.15 m).
[f] Terrestrial limiting point.

layer 4 of Blanc and Segre (1953), layer 6 of Durante and Settepassi (1974) and to the sample GDC-8 of Marra et al. (2023), which was dated to ≤106.4 ± 10.8 ka (Fig. 3). LU7 consists of reddish sandy sediments similar to underlying LU5, but with an enrichment of faintly stratified fine gravel (Fig. 2a). Moving toward this lateral entrance, LU7 gradually becomes thicker and shows richer and coarser component of limestone gravel (Fig. 2b). LU9 is a greyish-yellowish coarse tephra layer (Fig. 3). It is composed by strongly altered, whitish, up to 5 mm-sized, pumice fragments and abundant sanidine crystals. LU9 probably correspond to layer 10 of Blanc and Segre (1953), whereas it is unclear the correlation with Durante and Settepassi (1974). This sub-primary tephra layer was precisely dated by Marra et al. (2023) at 109.3 ± 0.5 ka, using the same monitor standard employed in Monaco et al. (2022), and correlated to the widespread Maddaloni/X-6 tephra (Marra et al., 2023), from Campi Flegrei caldera (Monaco et al., 2022). LU10 is again a stratified reddish silty sand with lenses of breccia and increasing of clastic material (Fig. 3). LU11 is a dark carbon rich sandy silt material containing lens of reworked volcanic ash (Fig. 3).

Blocks fall deposit (LU8) consists of blocks with few reddish matrix. The lower face of the blocks is characterized by abundant *Lithophaga* boreholes indicating that these blocks derive from the collapse of the ceiling (Fig. 3). This unit corresponds to layer 6 of Blanc and Segre (1953) and layer 5 of Durante and Settepassi (1974). The top of LU8 is characterized by an increase in the reddish matrix and a decrease in the size of clasts.

Finally, the upper part of the section is quite disturbed and covered by reworked historical material, as reported in previous studies (Ruffo and Zarattini, 1991). Therefore we did not include this surficial unit in the stratigraphic log.

4.2. U/Th dating

The sample GDC12 of the flowstones draping the notch and the *Lithophaga* boreholes at 9.51 ± 0.14 m a.s.l. yielded a very young age of 2.8 ± 0.3 ka (Table 1), thus not useful to constrain the age of these sea-level highstand morphological markers.

Three out of the eight U/Th ages obtained for the sample GDC5, from the stalagmite laying at the base of the clastic sedimentary infilling at 3.10 m a.s.l. (Fig. 3), are characterized by large clastic contamination (i.e., $^{230}Th/^{232}Th$ atomic ratio lower than 40, Table 1), and should thus be considered with caution. However, the five less contaminated samples yielded robust ages from the bottom to the top ranging from 122.8 ± 1.0 ka to 113.2 ± 2.2 ka (Fig. 3; Table 1).

The multiple dating ($n = 5$) of the stalagmite GDC9, from the thinly laminated calcite at the top of LU5 (Fig. 3), yielded, from the bottom to the top, statistically almost indistinguishable ages ranging from 112.1 ± 1.1 ka 109.8 ± 0.8 ka, indicating a rapid growth of the speleothem (Fig. 3; Table 1).

The sample GDC3 collected in the inner part of the cave and covering surficial marine gravels yielded very contaminated ages, but suggesting a very young age in agreement with the upper flowstone covering the entire succession, including the historical (Roman) archeological layers.

4.3. Tephrochronology

Unfortunately, glass preservation from tephra and the volcaniclastic layers identified along the section (LU4, LU6 and LU9) was very poor, which at WDS-EMPA resulted in very low analytical totals, completely unreliable for the geochemical fingerprint.

5. Discussion

5.1. Age and nature of the Grotta delle Capre relative sea-level highstand markers

The general stratigraphy of the cave and the nature of the sediments

indicate that the cave entrance was never completely closed as supported by the archeological remains along the whole succession (Ruffo and Zarattini, 1991) and the presence in the LU5 of remains of land snail shells of semi-forest habitat like *Pomatia elegant* (e.g., Ložek, 1990). The LU8, representing a phase of collapse of the cave ceiling (Fig. 3), may have obstructed the cave entrance, but the presence of LU9 above this unit in a more internal position, which is an almost primary tephra deposit, indicates that this obstruction, if any, was only partial and likely short in time. So, there is no evidence of potential missing of marine transgression or RSL oscillation during the considered period.

The tidal notch retreat point at 9.51 ± 0.14 m and the upper limit of the *Lithophaga* boreholes band (which roughly matches the elevation of the tidal notch retreat point), provide clear indications for the highest RSL in the cave. Lithophaga are more or less ubiquitous limestone-boring lamellibranchs (e.g., Laborel and Laborel-Deguen, 1996). *Lithophaga lithophaga* live in the range of the upper limit of the infralittoral zone down to more than −30 m (Laborel and Laborel-Deguen, 1996). However, considering that the highest concentration of boreholes is generally in the top few meters and, in microtidal environment, their upper limit is very close to the mean sea level (Pérès and Picard, 1964; Laborel and Laborel-Deguen, 1996; Rovere et al., 2015), they are considered a good indicator of past RSL (e.g., Ferranti et al., 2006; Rovere et al., 2016). Specifically, the upper limit should closely represent the Mean Low Water Spring (MLWS) that in the Mediterranean - and specifically in the area of Grotta delle Capre (data from Civitavecchia tidal station, https://www.mareografico.it/it/stazioni.html) is ca. 20–25 cm below the Mean Sea Level (MSL, Rovere et al., 2015, 2016), assuming a tidal range similar to today.

Similarly, the retreat point of tidal notches is used to identify the former sea-level (Trenhaile, 2015 and reference therein). In the Mediterranean, the notch profile is supposed to extend between the lowest and highest tidal levels with the retreat point near the mean sea-level (Pirazzoli and Evelpidou, 2013; Antonioli et al., 2015). Antonioli et al. (2018) correlated these two RSL markers with the LIG based on the close presence (e.g., Grotta del Fossellone, Fig. 1) of marine coastal deposits containing the typical "warm" guest gastropod *Thetystrombus latus*, which is also corroborated by the paleontological finding from Durante and Settepassi (1974) in the LU1 and the recent radioisotopic date of Marra et al. (2023) even in an indirect way. The slightly different elevation of the two markers, i.e., the retreat point of notch and upper limit of *Lithophaga* boreholes band, both considered as relatively precise indicators of RSL, is coherent with some observation of the notches in caves along the Tyrrhenian coast, the elevation of which results not identical to that of the notch along exposed cliffs (Carobene, 2015).

In agreement with the previous interpretations of the most recent studies (e.g., Antonioli et al., 2018; Marra et al., 2023), these morphological markers of the sea-level highstand can reasonably be associated with the beach deposits of LU1, which likely represent the sub-coeval sedimentary expression of the tidal notch. Though not supported by chronological data, as the flowstone samples draping the tidal notch (GDC-12) and the beach deposits (GDC-3) collected in the interior of the cave yielded useless indications (Table 1), this assumption appears fully consistent with the nature of submerged beach deposits of LU1 and with its elevation, which ranges from ~3 m, at the cave entrance, to ~7 m, in the innermost cave room (Fig. 2c). An important direct chronological constrain for the age of LU1 beach deposits, as well as for the entire Grotta delle Capre succession, is represented by the age of the lower speleothem (LU2) developed over the marine beach LU1, which represents a terrestrial limiting point and thus a *terminus ante quem* for the deposition of LU1. Therefore, assuming that the markers of the sea stationing at 9.51 ± 0.14 m are the morphological expressions of the sub-coeval LU1 beach deposits, the ages of LU2 indicate that this sea-level highstand is older than ~123 ka (Table 1, Fig. 3), which consequently can be identified as the LIG highstand (Fig. 4).

The whole infilling succession following the basal stalagmite deposition (LU2) shows unambiguous continental features, related to the transport and alternation of sandy-silt sediments from outside the cave (e.g., the colluvial-aeolian sediments of LU3, alluvial sediment of LU5-LU11 containing sub-primary tephra fall LU9) and inside processes like the collapse of ceiling blocks (LU8), and chemical deposition (speleothems LU2 and within LU5) (Ruffo and Zarattini, 1991) (Figs. 3 and 4). This indicates that there is no evidence of sea-level rising above 3 m a.s.l. younger than 123 ka, during the LIG or other MIS 5 substages. This is confirmed by the speleothem ages found in younger LU5, which grew between ~112 ka and ~ 110 ka, and of the sub-primary tephra LU9, dated to ~109 ka (Marra et al., 2023) (Figs. 3 and 4). In contrast, based on a different interpretation of the genesis of the alluvial deposits containing the tephra LU9/Maddaloni/X-6, i.e., as colluviated dune deposits, and on their correlation with beach deposits, cropping along the Pontine coast, dated at ~101 ka, Marra et al. (2023) suggest a second rising of the sea-level at ~2.5 m a.s.l. during the MIS 5c. However, such an interpretation conflicts with the clear alluvial nature of the deposits containing the tephra LU9.

5.2. Implications for the age and dynamic of the LIG Sea-level highstand

5.2.1. Comparison with other well-dated LIG and post-LIG records along the Tyrrhenian coasts

Despite the great wealth of morphological and sedimentary records associated with the LIG highstand preserved all over the Tyrrhenian coasts (e.g., Antonioli et al., 2018), relatively few archives hold a solid and high-resolution chronology required for reconstructing in detail the timing and dynamic of the RSL during the LIG. For instance, according to Pasquetti et al. (2021) the application of strict geochemical criteria to the U/Th samples of the LIG deposits indicates that only ~33% of data available for the Mediterranean Sea can be considered "reliable", but none are from the Tyrrhenian coast of Italian Peninsula. A specific case is the Infreschi Cave, in southern Campania, 200 km away from Grotta delle Capre (Fig. 1). Here a precise assessment of the LIG RLS dynamic (Bini et al., 2020) was obtained based on the same approach of dating terrestrial limiting points. Bini et al. (2020) found that, following a stationing at ~9 m a.s.l., marked by a well-developed upper horizontal level of *Lithophaga* boreholes at 8.7 ± 0.6 m a.s.l., the RSL dropped below ~3 m a.s.l. before 120 ka. Then a continental succession containing Middle Paleolithic artefacts with a thick tephra layer chemically correlated with the Mediterranean tephra marker X-6, dated at ~109 ka (e.g., Regattieri et al., 2015) and recently attributed to the Maddaloni eruption from an early activity of the Campi Flegrei caldera (Monaco et al., 2022), complete the successions. Therefore, overall, the Infreschi Cave and Grotta delle Capre replicate the same sequence of sub-synchronous - within the chronological uncertainty - events. In particular, despite the lack of geochemical data for the tephra LU9 from Grotta delle Capre, its $^{40}Ar^{39}Ar$ dating, indistinguishable from that of Maddaloni/X-6 (i.e., 109.5 ± 0.5 ka and 109.3 ± 1.0 ka, respectively), strongly support the correlation of the tephra LU9 with the Maddaloni/X-6 (Marra et al., 2023), so allowing a direct tephra synchronization with Infreschi Cave and adding a new point of occurrence of this well-known and widespread marker for the MIS 5 successions in the Central Mediterranean area (Zanchetta et al., 2018; Monaco et al., 2022). Summarising, Infreschi and Capre appear to have undergone a similar morpho-sedimentary evolution, providing convergent evidence that on the eastern coasts of the Tyrrhenian Sea, as early as 123–120 ka, the RSL was well below ~3 m a.s.l., with an important sea-level drop of at least 5–6 m occurring between the maximum LIG highstand, and before 123–120 ka.

Geochronological constraints were recently also acquired for the marine and continental sedimentary infilling of the Guattari Cave (Marra et al., 2023; Rolfo et al., 2023), a few kilometers away from Grotta delle Capre (Fig. 1). This set of chronological data is based on the $^{40}Ar/^{39}Ar$ dating of detrital sanidine, which provides a *terminus post quem* for the sediment from which the sanidine crystals are extracted. The sanidine from the basal marine deposits containing *Thetystrombus*

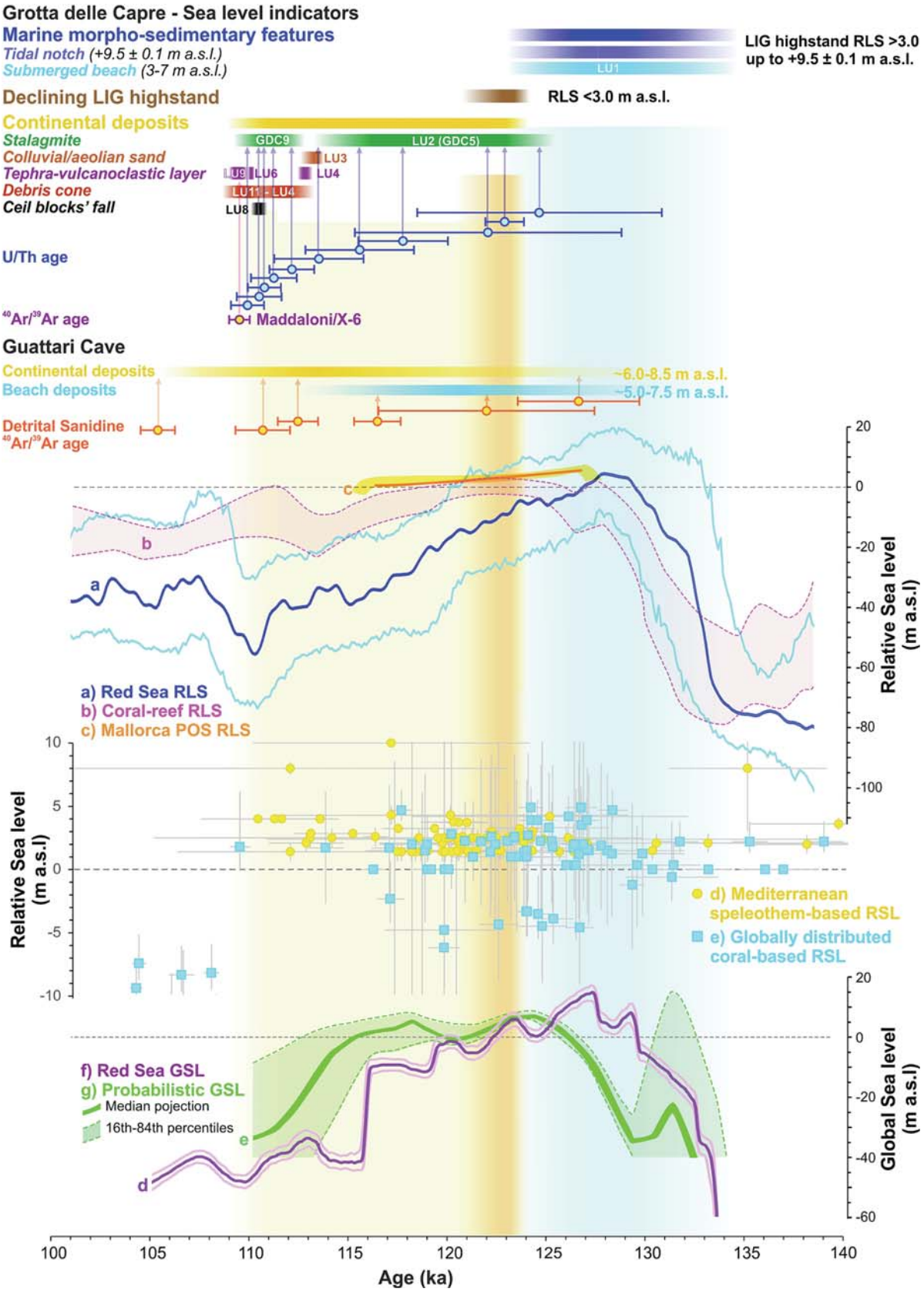

(caption on next page)

Fig. 4. Paleoenvironmental history and relative sea-level (RSL) indicators from Grotta delle Capre and nearby Guattari Cave (Marra et al., 2023, Rolfo et al., 2023; Fig. 1) compared with global and Mediterranean reference records. The $^{40}Ar/^{39}Ar$ age for the tephra LU9, correlated to the Maddaloni/X-6 marker tephra, is from Marra et al. (2023). a) Red Sea RSL record (dark blue curve) and the associated uncertainty (pale blue curves) from Grant et al. (2012, 2014); b) Monte Carlo 95% confidence interval of selected U/Th dating ($\delta^{234}U_i$ 137–157‰) of sea-level markers from global coral reefs (Medina-Elizalde, 2013); c) Mediterranean RSL from Mallorca Island, based on phreatic overgrowth stalagmite (POS) corrected for GIA (Polyak et al., 2018); d) Mediterranean RSL based on U/Th dating of terrestrial speleothems and phreatic overgrowths on speleothems that passed geochemical screening proposed by Pasquetti et al. (2021); e) Globally distributed RSL records based on U/Th dating of corals that passed the geochemical screening proposed by Hibbert et al. (2016); f) Global Mean Sea Level (GMSL) approximation based from Red Sea core KL11 PM (purple blue line) and its 95% probability interval (purple blue lines) (modified after Rohling et al., 2019); g) probabilistic assessment of the global sea-level based on statistical analyses of several globally distributed records (Kopp et al., 2009). (For interpretation of the references to colour in this figure legend, the reader is referred to the web version of this article.)

latus at ~5 m a.s.l. and from a patch of marine sand cemented to the cave ceiling at ~7.50 m a.s.l., provided the age of 121.7 ± 5.8 ka 116.2 ± 1.2 ka, respectively. The sanidine from the sandy continental deposit laying on the LIG beach yielded instead the age of 126.4 ± 3.0 ka, 112.1 ± 1.0 ka, 110.4 ± 1.4 ka, 104.9 ± 0.9 ka and 101.0 ± 9.2 ka. Overall, these data support the attribution of the beach deposits to the LIG highstand but indicate that the sea-level was not lower than ~7.50 m a.s.l. until 116 ka, at least (Fig. 4), thus not in agreement with the early end of the LIG sea-level highstand documented at Grotta delle Capre and Infreschi Cave.

5.2.2. *The Grotta delle Capre RSL record in the framework of the regional and global reference successions*

Comparing our RSL values with regional or global data obtained from "far field" sites (e.g., Chen et al., 1991; Stirling et al., 1998; Medina-Elizalde, 2013), and other reference records (e.g., the Red Sea, Rohling et al., 2019), is challenging for the different GIA correction and potential tectonic biases, which can exist between sites. Aware of these limits and of the local meaning of the Grotta delle Capre and Infreschi Cave RSL records, we notice that the early fall of the LIG sea-level at 123–120 ka documented at these sites does not agree with some chronologically well-constrained Mediterranean records of the LIG RSL (e.g., Pasquetti et al., 2021). In particular, direct U/Th dating of corals *Cladocora caespitosa* from the Balearic Island of Mallorca (Muhs et al., 2015) indicates an age ranging from ~126 to ~118 ka for the LIG highstand corresponding to a RSL of 2.10 ± 0.71 m a.s.l. (Lorscheid et al., 2017) (Fig. 4). This is in good agreement with the detrital sanidine $^{40}Ar/^{39}Ar$ chronology of the nearby Guattari Cave (Marra et al., 2023), the U/Th chronology of phreatic overgrowth on speleothems that date the LIG highstand between 126.6 ± 0.4 ka and 116.0 ± 0.8 ka, with a RSL at 2.15 ± 0.75 m a.s.l. (Polyak et al., 2018) and with the globally distributed coral-based evidence supported by a U/Th chronology that passed a restrictive geochemical screening (Hibbert et al., 2016) (Fig. 4), even if coral-based RSL reconstruction can have a large associate error in RSL estimation (Fig. 4).

In contrast, other studies indicate a short duration for the peak of the LIG highstand and/or a more complex dynamic of the LIG highstand, featured by several oscillations (e.g., Grant et al., 2012, 2014; Kopp et al., 2009; Rohling et al., 2019; Medina-Elizalde, 2013), which is in agreement with our data. Specifically, according to the "empirical" isotopic-based RSL curve proposed by Rohling et al. (2019), the LIG sea-level highstand was featured by several oscillations since ~129 ka to ~122 ka (Fig. 4), thus consistent with Capre and Infreschi evidence. Instead, the probabilistic assessment of the sea level during the LIG, based on statistical analyses of several globally distributed records (Kopp et al., 2009), shows two distinct peaks of the LIG highstand occurring at 126–121 ka and 119–115 ka, respectively (Fig. 4). However, while for the early peak at ~124 ka there is a 95% probability that the sea-level was between 3.5 m and 10.0 m a.s.l., during the later peak at ~118 ka there is a 95% probability that it was between −9 and 10 m a.s.l. (Fig. 4). Therefore, the elevation of the later sea level highstand peak is associated with a substantially higher uncertainty than the older one, and there is a significant probability that it was substantially lower than the earlier peak or even below the present sea-level (Fig. 4). In this regard, and in a very general sense, without specific consideration of GIA, the morphostratigraphic and chronological evidence from Grotta delle Capre, indicating that after 123 ka the sea-level definitively fell at elevations <3 m a.s.l., is in agreement with the uncertainty associated with the second LIG RLS peak, in fact suggesting that on the Tyrrhenian coasts of central Italy this possible later LIG sea-level rise would have not occurred and in any case would have not exceeded this height (Fig. 4).

Several numerical GIA models indicate that the RSL highstand could have occurred in many sectors of the Mediterranean at different times and elevations (Antonioli et al., 2018; Stocchi et al., 2018; Bini et al., 2020). According to Antonioli et al. (2018) in the tectonically stable areas of the Mediterranean, the elevation of the LIG highstand, indicated by tidal notches, ranges from ~2 to ~12 m a.s.l., with a mean of 5.7 m a.s.l. Such variability was interpreted as small land movements, deriving from slow crustal processes, which occurred also in apparently more stable areas. Antonioli et al. (2018) compared these altitudinal differences against GIA model predictions from a suite of ice-sheet models. In particular, they used here different GIA models: (i) ICE-5G, of Peltier (2004), is a model that describes the ice-sheet thickness variations over North America, Eurasia, Greenland and Antarctica from 26 ka to present. For this time span, ICE-5G was constrained by the means of geological RSL data and modern geodetic observations (Peltier, 2004). Prior to 26 ka, the ice-sheet growth is tuned to the $\delta^{18}O$ curve of Lisiecki and Raymo (2005). (ii) CE-6G is instead an implementation of the ICE-5G model (Peltier et al., 2015). Finally, (iii) ANICE-SELEN (e.g. de Boer et al., 2017) describes the global ice-sheet fluctuations that follow the $\delta^{18}O$ curve of Lisiecki and Raymo (2005) stack and that dynamically account for all the GIA feedback.

Their results indicated that the GIA signal is not the main cause of the observed highstand variability and that other mechanisms are involved. Interestingly, Antonioli et al. (2018) recalculated the predicted elevation between ~120 ka and ~115 ka using the ANICE-SELEN model (Fig. 5), which, at least in terms of the maximum LIG RSL elevation, is in relatively good agreement with the RSL highstand markers at Grotta delle Capre.

Specifically, the modelled data indicate that the predicted RSL elevation for Grotta delle Capre and Infreschi Cave is at ~8 m, i.e., slightly lower than the elevation of the RSL markers measured at both sites. These small differences can be accounted by model inaccuracy and/or the previously mentioned tectonic movements. However, the same ANICE-SELEN model suggests that maximum RLS was reached quite late during the LIG, between 120 and 117 ka (Fig. 5), thus in contrast with the replicated and stratigraphically robust chronological data from Grotta delle Capre and Infreschi Cave indicating that at ~120–123 ka RSL had already dropped below ~3 m a.s.l (Fig. 5). Moreover, the ANICE-SELEN model, though reproducing quite well the second, but not well-constrained, sea level rise during the second half of the LIG, fails in reproducing the earlier and statistically well-constrained peak of the LIG highstand, as reconstructed by Kopp et al. (2009) (Fig. 5). On the contrary, as the ICE-6G and ICE-5G RSL modelled curves are concerned, if on one hand they appear in agreement with our chronological data, i.e., they predict a similar early fall of the sea-level at ~122–120 ka, on the other they fail in reproducing the magnitude of the local RSL, as they predict a maximum RLS of only 4 m a.s.l. (Fig. 5). These mismatching can be accounted for the obvious differences in the input data and boundary conditions of the models. With this regard, our

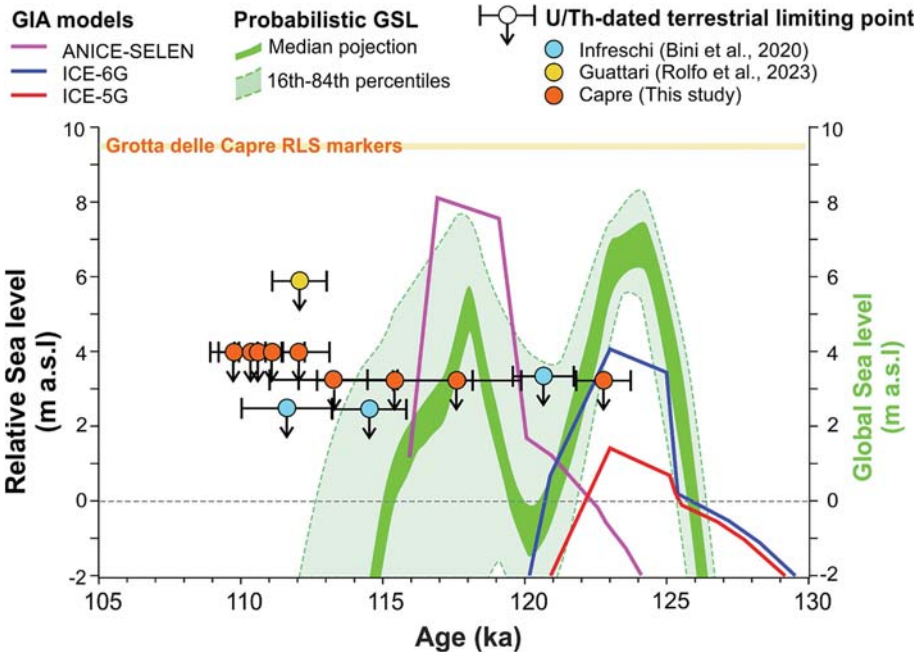

Fig. 5. Comparison between selected, high-precision and high $^{230}Th/^{232}Th$ activity ratio (>40; i.e., little age correction) of terrestrial limiting points from Italian coastal caves on Tyrrhenian Sea (Grotta delle Capre, this study; Infreschi Cave, Bini et al., 2020; Guattari Cave, Rolfo et al., 2023), the GIA models ANICE-SELEN (Antonioli et al., 2018); ICE-6G and ICE-5G (Peltier et al., 2015; Peltier, 2004) and the global sea-level record from Kopp et al. (2009).

data may provide useful constraints to reduce the degree of assumptions and the uncertainties of the input data and thus helping their improvements.

6. Summary and concluding remarks

A new survey at Grotta delle Capre confirms that there are two main sea-level markers, represented by a clear retreat point of the notch and the upper limit of *Lithophaga* borehole band at ~9.5 m a.s.l., interpreted as indicators of the highstand during the LIG. These sea-level indicators appear to be associated with a beach deposit, the depositional top surface of which ranges in elevation from ~3 m a.s.l., at the cave entrance, to ~7 m a.s.l., in the innermost cave room. A suite of U/Th dating of a speleothem growth directly on this marine unit at an elevation of ~3 m a.s.l. indicates that the influence of the sea was no longer recorded in the cave after ~123 ka, and that before this age the RSL dropped by 6 m at least. This basal speleothem is in turn covered by a 4.5 m-thick succession of continental deposits, containing a second speleothem laying at ~4 m a.s.l., dated by U/Th methods to be between ~112 ka and 110 ka, and the Mediterranean tephra marker Maddaloni/X-6 of ~109 ka, which indicates that no further sea-level oscillation >3 m during the LIG is recorded in Grotta delle Capre.

Overall, our data support the notion of very short duration sea-level LIG highstand and of a likely rapid drop from ~9 m a.s.l. to <3 m. a.s.l. before ~123 ka. This is in agreement with previous stalagmite evidence indicating that along the Tyrrhenian coast the RSL during the LIG highstand dropped for several meters at some time between its maximum height, presumably in the interval 129–123 ka, and prior to 120 ka (Bini et al., 2020). These data are in good agreement with the probabilistic assessment of the global sea-level by Kopp et al. (2009) and with the RSL curve proposed by Rohling et al. (2019), both showing a complex history of the sea-level variations, with at least two prominent oscillations within the LIG. Specifically, our data fit very well with the early (126–120 ka) statistically more robust peak of the LIG global sea-level of Kopp et al.'s (2009) reconstruction, while they indicate that the late peak (119–115 ka), which is associated with a higher uncertainty, if occurred, on the Tyrrhenian coast did not exceed the height of 3 m a.s.l. On the contrary, the present and previous U/Th-dated terrestrial limiting points of the LIG highstand on Tyrrhenian coasts are not completely captured by the model output proposed in Antonioli et al. (2018) and suggest a shorter duration of the highstand compared, for instance, with data from Mallorca Island in the western Mediterranean. Our results and their comparison with evidence from the literature evidence confirm that the overall framework of the LIG sea-level dynamic is extremely complex and far from being a coherent one. More high-resolution stratigraphic and chronological investigations are thus needed to reduce uncertainties in reconstructing the LIG RSL records and in GIA numerical models, which are fundamental for understanding the cryosphere and sea-level dynamics during this warm period, also as a potential long-term scenario of the future sea-level rise under the current global warming.

Declaration of Competing Interest

The authors declare that they have no known competing financial interests or personal relationships that could have appeared to influence the work reported in this paper.

Data availability

Data will be made available on request.

Acknowledgments

U/Th dating was supported by grants from the Ministry of Science and Technology (MOST) and National Science and Technology Council, Taiwan, ROC (110-2123-M-002-009 and 111-2116-M-002-022-MY3 to C.-C.S.), the Higher Education Sprout Project of the Ministry of Education, Taiwan, ROC (110L901001 to C.-C.S.), the National Taiwan University (112L894202 to C.-C.S.). GZ and MB are funded by University of Pisa, through "Ateneo Funding". We thank two anonymous reviewers for their useful comment.

Appendix A. Supplementary data

Supplementary data to this article can be found online at https://doi.org/10.1016/j.gloplacha.2023.104321.

References

Alley, R.B., Clark, P.U., Huybrechts, P., Joughin, I., 2005. Ice-sheet and sea-level changes. Science 310, 456–460.

Antonioli, F., Lo Presti, V., Rovere, A., Ferranti, L., Anzidei, M., Furlani, S., Mastronuzzi, G., Orru, P.E., Scicchitano, G., Sannino, G., Spampinato, C.R., Pagliarulo, R., Deiana, G., de Sabata, E., Sansò, P., Vacchi, M., Vecchio, A., 2015. Tidal notches in Mediterranean Sea: a comprehensive analysis. Quat. Sci. Rev. 119, 66–84.

Antonioli, F., Ferranti, L., Stocchi, P., Deiana, G., Lo Presti, V., Furlani, S., Marino, C., Orru, P., Scicchitano, G., Trainito, E., Anzidei, M., Bonamini, M., Sansò, P., Mastronuzzi, G., 2018. Morphometry and elevation of the last interglacial tidal notches in tectonically stable coasts of the Mediterranean Sea. Earth-Sci. Rev. 185, 600–623.

Barlow, N.L.M., McClymont, E.L., Whitehouse, P.L., Stokes, C.R., Jamieson, S.S.R., Woodroffe, S.A., Bentley, M.J., et al., 2018. Lack of evidence for a substantial sealevel fluctuation within the last interglacial. Nat. Geosci. 11 (9), 627e634.

Bietti, A., Grimaldi, S., 1991. Patterns of reduction sequences at Grotta Breuil: statistical analyses and comparisons of archaeological vs. experimental data. Quatern. Nova 1, 379–406.

Bini, M., Isola, I., Zanchetta, G., Pappalardo, M., Ribolini, A., Ragaini, L., Baroni, C., Boretto, G., Fuck, E., Morigi, C., Salvatore, M.C., Bassi, D., Marzaioli, F., Terrasi, F., 2018. Middle Holocene relative sea-level along Atlantic Patagonia: new data from Camarones (Chubut, Argentina). The Holocene 28, 56–64.

Bini, M., Zanchetta, G., Drysdale, R.N., Giaccio, B., Stocchi, P., Vacchi, M., Hellstrom, J. C., Couchoud, I., Monaco, L., Ratti, A., Martini, F., Sarti, L., 2020. An end to the Last Interglacial highstand before 120 ka: relative sea-level evidence from Infreschi Cave (Southern Italy). Quat. Sci. Rev. 250, 106658 https://doi.org/10.1016/j.quascirev.2020.106658.

Blanc, A.C., Segre, A.G., 1953. Le Quaternaire du Monte Ciceo. Livr. Guide IV Congr, INQUA Roma.

Bonifay, E., Mars, P., 1959. Le Tyrrhénien dans le cadre de la chronologie quaternaire méditeranéenne. Bull. Soc. Geol. Fr. 7, 62–78.

Burke, K.D., Williams, J.W., Chandler, M.A., Haywood, A.M., Lunt, D.J., Otto-Bliesner, B. L., 2018. Pliocene and Eocene provide best analogs for near-future climates. PNAS 115, 13288–13293.

CAPE-Last Interglacial Project Members, 2016. Last Interglacial Arctic warmth confirms polar amplification of climate change. Quat. Sci. Rev. 25, 1383–1400.

Capron, E., Rovere, A., Austermann, J., Axford, Y., Barlow, N.L.M., Carlson, A.E., de Vernal, A., Dutton, A.i., Kopp, R.E., McManus, J.F., Menviel, L., Otto-Bliesner, B.L., Robinson, A., Shakun, J.D., Tzedakis, P.C., Wolff, E.C., 2019. Challenges and research priorities to understand interactions between climate, ice sheets and global mean sea level during past interglacials. Quat. Sci. Rev. 219, 308–311.

Carobene, L., 2015. Marine notheces and sea-cave bioerosional grooves in microtidal areas: examples from the Tyrrhenian and Ligurian Coasts-Italy. J. Coast. Res. 31, 536–556.

Cerrone, C., Vacchi, M., Fontana, A., Rovere, A., 2021. Last Interglacial sea-level proxies in the western Mediterranean. Earth Syst. Sci. Data 13, 4485–4527.

Chen, J.H., Curran, H.A., White, B., Wasserburg, G.J., 1991. Precise chronology of the last interglacial period: 234U/230Th data from fossil coral reefs in the Bahamas. Geol. Soc. Am. Bull. 103, 82–97.

Cheng, H., Lawrence Edwards, R., Shen, C.C., Polyak, V.J., Asmerom, Y., Woodhead, J., Hellstrom, J.H., Wang, Y., Kong, X., Spötl, C., Wang, X., Calvin, A.E., 2013. Improvements in ^{230}Th dating, ^{230}Th and ^{234}U half-life values, and U-Th isotopic measurements by multi-collector inductively coupled plasma mass spectrometry. Earth Planet. Sci. Lett. 371–372, 82–91.

Clark, P.U., Huybers, P., 2009. Interglacial and future sea level. Nature 462, 856–857.

de Boer, B., Stocchi, P., Whitehouse, P.L., van de Wal, R.S.W., 2017. Current state and future perspective on coupled ice-sheet - sea-level modeling. Quat. Sci. Rev. 169, 13–28.

Dumitru, O.A., Polyak, V.J., Asmerom, Y., Onac, B.P., 2021. Last interglacial sea-level history from speleothems: a global standardized database. Earth Syst. Sci. Data 13, 2077–2094.

Durante, S., 1975. Sul Tirreniano e la malacofauna della Grotta del Fossellone (Circeo). Quaternaria 18, 331–345.

Durante, S., Settepassi, F., 1974. Livelli marini e molluschi tirreniani alla Grotta delle Capre. Memorie dell'Istituto Italiano di Paleontologia Umana 2, 285–296.

Dutton, A., Carlson, A.E., Long, A.J., Milne, G.A., Clarck, P.U., De Conto, R., Horton, B.P., Rahmstorf, S., Raymo, R.E., 2015. Sea-level rise due to polar ice-sheet mass loss during past warm periods. Science 349 (6244), aaa4019.

Dyer, B., Austermann, J., D'Andrea, W.J., Creel, R.C., Sandstrom, M.R., Cashman, M., Rovere, A., Raymo, M.E., 2021. Sea-level trends across the Bahamas constrain peak last interglacial ice melt. Proc. Natl. Acad. Sci. USA 17 (33), 118.

Ferranti, L., Antonioli, F., Mauz, B., Amoros, i A., Dai Pra, G., Mastronuzzi, G., Monaco, C., Orrù, P., Pappalardo, M., Radke, U., Renda, P., Romano, P., Sansò, P., Verrubbi, V., 2006. Markers of the last interglacial sea-level high stand along the coast of Italy: Tectonic implications. Quat. Int. 145–146, 30–54.

Frisia, S., Borsato, A., Fairchild, I.J., McDermott, F., 2000. Calcite fabrics, growth mechanisms, and environments of formation in speleothems from the Italian Alps and southwestern Ireland. J. Sediment. Res. 70 (5), 1183–1196.

Govin, A., Capron, E., Tzedakis, P.C., Verheyden, S., Ghaleb, B., Hillaire-Marcel, C., St-Onge, G., Stoner, J.S., Bassinot, F., Bazin, L., Blunier, T., Combourieu-Nebout, N., El Ouahabi, A., Genty, D., Gersonde, R., Jimenez-Amat, P., Landais, A., Martrat, B., Masson-Delmotte, V., Parrenin, F., Seidenkrantz, M.-S., Veres, D., Waelbroeck, C., Zahn, R., 2015. Sequence of events from the onset to the demise of the Last Interglacial: evaluating strengths and limitations of chronologies used in climatic archives. Quat. Sci. Rev. 129, 1–36.

Grant, K.M., Rohling, E.J., Bar-Matthews, M., Ayalon, A., Medina-Elizalde, M., Ramsey, C.B., Satow, C., Roberts, A.P., 2012. Rapid coupling between ice volume and polar temperature over the past 150,000 years. Nature 491 (7426), 744–747.

Grant, K.M., Rohling, E.J., Bronk Ramsey, C., Cheng, H., Edwards, R.L., Florindo, F., Heslop, D., Marra, F., Roberts, A.P., Tamisiea, M.E., Williams, F., 2014. Sea-level variability over five glacial cycles. Nat. Commun. 5, 5076.

Hearty, P.J., Miller, G.H., Stearns, C., Szabo, B.J., 1986. Aminostratigraphy of Quaternary shorelines around the Mediterranean basin. Geol. Soc. Am. Bull. 97, 850–858.

Hearty, P.L., Hollin, J.T., Neumann, A.C., O'Leary, M.J., McCulloch, M., 2007. Global sea-level fluctuations during the last Interglaciation (MIS5e). Qua. Sci. Rev. 26, 2090–2112.

Hibbert, F.D., Rohling, E.J., Dutton, A., Williams, F.H., Chutcharavan, P.M., Zhao, C., Tamisiea, M.E., 2016. Coral indicators of past sea-level change: a global repository of U-series dated benchmarks. Quat. Sci. Rev. 145, 1–56.

Hillaire-Marcel, C., Gariépy, C., Ghaleb, B., Goy, J.L., Zazo, C., Barcelo, J.C., 1996. U series measurements in Tyrrhenian deposits from mallorca - further evidence for two last-interglacial high sea levels in the Balearic Islands. Quat. Sci. Rev. 15, 53–62.

Hoffman, J.S., Clark, P.U., Parnell, A.C., He, F., 2017. Regional and global sea-surface temperatures during the last interglaciation. Science 355, 276–279.

IPCC, 2023. Sections. In: Core Writing Team, Lee, H., Romero, J. (Eds.), Climate Change 2023: Synthesis Report. Contribution of Working Groups I, II and III to the Sixth Assessment Report of the Intergovernmental Panel on Climate Change. IPCC, Geneva, Switzerland, pp. 35–115. https://doi.org/10.59327/IPCC/AR6-9789291691647.

Issel, A., 1883. Grotta delle Capre. In: Le Oscillazioni lente del suolo o bradisismi, pp. 205–210. Genova.

Jaffey, A.H., Flynn, K.F., Glendenin, L.E., Bentley, W.T., Essling, A.M., 1971. Precision measurement of half-lives and specific activities of U 235 and U 238. Physical Review C 4 (5), 1889.

Joughin, I., Alley, R.B., 2011. Stability of the West Antarctic ice sheet in a warming world. Nat. Geosci. 4, 506–513.

Kopp, R.E., Simons, F.J., Mitrovica, J.X., Maloof, A.C., Oppenheimer, M., 2009. Probabilistic assessment of sea level during the last interglacial stage. Nature 462, 863–867.

Laborel, J., Laborel-Deguen, F., 1996. Biological indicators of Holocene sea-level and climatic variations on rocky coasts of tropical and subtropical regions. Quat. Int. 31, 53–60.

Levermann, A., Clark, P.U., Marzeion, B., Milne, G.A., Pollard, D., Radic, V., Robinson, A., 2013. The multimillennial sea-level commitment of global warming. PNAS 110, 13745–13750.

Lisiecki, L., Raymo, M., 2005. A Pliocene-Pleistocene stack of 57 globally distributed benthic δ18O records. Paleoceanography 20 (2), PA1003.

Lorscheid, T., Stocchi, P., Casella, E., Gomez-Pujol, L., Vacchi, M., Mann, T., Rovere, A., 2017. Paleo sea-level changes and relative sea-level indicators: precise measurements, indicative meaning and glacial isostatic adjustment perspectives from Mallorca (Western Mediterranean). Palaeogeogr. Palaeoclimatol. Palaeoecol. 473, 94–107.

Ložek, V., 1990. Molluscs in loess, their paleoecological significance and role in geochronology principals and methods. Quat. Int. 7 (8), 71–79.

Lüthi, D., Le Floch, M., Bereiter, B., Blunier, T., Barnola, J.-M., Siegenthaler, U., Raynaud, D., Jouzel, J., Fischer, H., Kawamura, K., Stocker, T.F., 2008. High-resolution carbon dioxide concentration record 650,000–800,000 years before present. Nature 453, 379–382.

Marra, F., Bahain, J.-J., Jicha, B.R., Nomade, S., Palladino, D.M., Pereira, A., Tolomei, C., Pierre Voinchet, P., Anzidei, M., Aureli, D., Ceruleo, P., Falgueres, C., Florindo, F., Gatta, M., Ghaleb, B., La Rosa, M., Peretto, C., Petronio, C., Rocca, R., Rolfo, M.F., Salari, L., Smedile, A., Tombret, O., 2019. Reconstruction of the MIS 5.5, 5.3 and 5.1 coastal terraces in Latium (central Italy): a re-evaluation of the sea-level history in the Mediterranean Seaduring the last. Quat. Int. 525, 54–77.

Marra, F., Rolfo, F.M., Gaeta, M., Florindo, F., 2020. Anomalous Last Interglacial Tyrrhenian Sea levels and Neanderthal settling at Guattari and Moscerini Caves (central Italy). Sci. Rep. 10 (1), 11929. https://doi.org/10.1038/s41598-020-68604-z.

Marra, F., Florindo, F., Gaeta, M., Jicha, B.R., 2023. ^{40}Ar/^{39}Ar age constraints on MIS 5.5 and MIS 5.3 paleo-sea levels: Implications for global sea levels and ice-volume estimates. Paleoceanogr. Paleoclimatol. https://doi.org/10.1029/2023PA004679 e2023PA004679.

Mauz, B., 1999. Late Pleistocene records of littoral processes at the Tyrrhenian Coast (Central Italy): depositional environments and luminescence chronology. Quat. Sci. Rev. 18, 1173–1184.

Medina-Elizalde, M., 2013. A global compilation of coral sea-level benchmarks: Implications and new challenges. Earth Planet. Sci. Lett. 362, 310–318.

Monaco, L., Palladino, D.M., Albert, P.G., Arienzo, I., Conticelli, S., Di Vito, M., Fabbrizio, A., D'Antonio, M., Isaia, R., Manning, C.J., Nomade, S., Pereira, A., Petrosino, P., Sottili, G., Sulpizio, R., Zanchetta, G., Giaccio, B., 2022. Linking the

Mediterranean MIS 5 tephra markers to Campi Flegrei (southern Italy) 109–92 ka explosive activity and refining the chronology of MIS 5c-d millennial-scale climate variability. Global Planet. Change 211, 103785.
Muhs, D.R., 2002. Evidence for the timing and duration of the Last Interglacial period from high-precision uranium- series ages of corals on tectonically stable coastlines. Quatern. Res. 58, 36–40.
Muhs, D.R., Simmons, K.R., Meco, J., Porat, N., 2015. Uranium-series ages of fossil corals from Mallorca, Spain: the "Neotyrrhenian" high stand of the Mediterranean Sea revisited. Palaeogeogr. Palaeoclimatol. Palaeoecol. 438, 408–424.
O'Leary, M.J., Hearty, P.J., Thompson, W.G., Raymo, M.E., Mitrovica, J.X., Webster, J. M., 2013. Ice sheet collapse following a prolonged period of stable sea level during the last interglacial. Nat. Geosci. 6, 796–800.
Otto-Bliesner, B.L., Marshall, S.J., Overpeck, J.T., Miller, G.H., Hu, A., CAPE, 2006. Last Interglacial Proect members - simulating arctic climate warmth and icefield retreat in the Last Interglaciation. Science 311, 1751–1753.
Pasquetti, F., Bini, M., Giaccio, B., Vacchi, M., Zanchetta, G., 2021. Chronology of the Mediterranean sea-level highstand during the Last Interglacial: a critical review of the U/Th-dated deposits. J. Quat. Sci. 36, 1174–1189.
Past Interglacials Working Group of PAGES, 2016. Interglacials of the last 800,000 years. Rev. Geophys. 54 https://doi.org/10.1002/2015RG000482.
Peltier, W.R., 2004. Global glacial isostasy and the surface of the ICE-age earth: the ICE-5G (VM2) model and GRACE. Annu. Rev. Earth Planet. Sci. 32, 111–149.
Peltier, W.R., Argus, D.F., Drummond, R., 2015. Space geodesy constrains ICE age terminal deglaciation, the global ICE-6G_C (VM5a) model. J. Geophys. Res. Solid Earth 120, 450–487.
Pérès, J.M., Picard, J., 1964. Nouveaou Manuel de Bionomie Benthique de la Mer Mediterranee. Rec. Trav. Stat. Mar. Endoume 31, 137 pp.
Pirazzoli, P.A., Evelpidou, N., 2013. Tidal notches: a sea-level indicator of uncertain archival trustworthiness. Palaeogeogr. Palaeoclimatol. Palaeoecol. 369, 377–384.
Polyak, V.J., Onac, B.P., Fornos, J.J., Hay, C., Asmerom, Y., Dorale, J.A., Gines, J., Tuccimei, P., Gines, A., 2018. A highly resolved record of relative sea level in the western Mediterranean Sea during the last interglacial period. Nat. Geosci. 11, 860–864.
Regattieri, E., Giaccio, B., Zanchetta, G., Drysdale, R.N., Galli, P., Nomade, S., Peronace, E., Wulf, S., 2015. Hydrological variability over Apennine during the Early Last Glacial precession minimum, as revealed by a stable isotope record from Sulmona basin, central Italy. J. Quat. Sci. 30, 19–31.
Rohling, E.J., Grant, K., Hemleben, Ch., Siddall, M., Hoogakker, B.A.A., Bolshaw, M., Kucera, M., 2009. High rates of sea-level rise during the last interglacial period. Nat. Geosci. 1, 38–42.
Rohling, E.J., Hibbert, F.D., Grant, K.M., Galaasen, E.V., Irvali, N., Kleiven, H.F., Marino, G., Ninnemann, U., Roberts, A.P., Rosenthal, Y., 2019. Asynchronous Antarctic and Greenland ice-volume contributions to the last interglacial sea level highstand. Nat. Commun. 10, 5040. https://doi.org/10.1038/s41467-019- 12874-3.
Rolfo, M.F., Bini, M., Di Mario, F., Ferracci, A., Giaccio, B., Hsun-Ming, H., Isola, I., Sadori, L., Shen, C.-C., Vignola, C., Zanchetta, G., 2023. Neanderthal bones collected by hyena at Grotta Guattari, central Italy, 66–65 ka: U/Th chronology and paleoenvironmental setting. Quat. Sci. Rev. 311, 108132.
Rovere, A., Antonioli, F., Bianchi, C.N., 2015. Chapter 18. Fixed biological indicators. In: Shennan, A., Horton, B.P. (Eds.), Handbook of Sea-Level Research. Wiley & Sons Ltd., pp. 268–280
Rovere, A., Raymo, M.E., Vacchi, M., Lorscheid, T., Stocchi, P., Gómez-Pujol, L., Harris, D.L., Casella, E., O'Leary, M.J., Hearty, P.J., 2016. The analysis of Last Interglacial (MIS 5e) relative sea-level indicators: reconstructing sea-level in a warmer world. Earth Sci. Rev. 159, 404–427.
Rovere, A., Ryan, D.D., Vacchi, M., Dutton, A., Simms, A.R., Murray-Wallace, C.V., 2023. The world atlas of last interglacial shorelines (version 1.0). Earth Syst. Sci. Data 15, 1–23.
Ruffo, M., Zarattini, A., 1991. The Grotta delle Capre (Goat Cave) at San Felice Circeo, further investigations. Quatern. Nova 1, 241–266.
Segre, A.G., 1991. Geomorphologie et Stratigraphie de la grotte Guattari au Mont Circe (Latina). Quatern. Nova 1, 97–106.
Shen, C.-C., Cheng, H., Edwards, R.L., Moran, S., Bedmonds, H.N., Hoff, J.A., Thomas, R. B., 2003. Measurement of attogram quantities of ^{231}Pa in dissolved and particulate fractions of seawater by isotope dilution thermal ionization mass spectroscopy. Anal. Chem. 75, 1075–1079.
Shen, C.-C., Li, K.-S., Sieh, K., Natawidjaja, D., Cheng, H., Wang, X., Edwards, R.L., Lam, D.D., Hsieh, Y.-T., Fan, T.-Y., Meltzner, A.J., Taylor, F.W., Quinn, T.M., Chiang, H.-W., Kilbourne, K.H., 2008. Variation of initial ^{230}Th/^{232}Th and limits of high precision U-Th dating of shallow-water corals. Geochim. Cosmochim. Acta 72, 4201–4223.
Shen, C.-C., Wu, C.-C., Cheng, H., Lawrence Edwards, R.L., Hsieh, Y.-T.S., Chang, C.-C., Li, T.-Y., Lam, D.D., Kano, A., Hori, M., Spötl, C., 2012. High-precision and high-resolution carbonate ^{230}Th dating by MC-ICP-MS with SEM protocols. Geochim. Cosmochim. Acta 99, 71–86.
Shennan, I., Long, A.J., Horton, B.P., 2015. Handbook of Sea-Level Research. John Wiley & Sons, Hoboken, NJ, p. 63.
Stirling, C.H., Esat, T.M., Lambeck, K., McCulloch, M.T., 1998. Timing and duration of the last interglacial; evidence for a restricted interval of widespread coral reef growth. Earth Planet. Sci. Lett. 160, 745–762.
Stocchi, P., Vacchi, V., Lorscheid, T., de Boer, B., Simms, A.R., van de Wal, R.S.W., Vermeersen, B.L.A., Pappalardo, P., Rovere, A., 2018. MIS 5e relative sea-level changes in the Mediterranean Sea: contribution of isostatic disequilibrium. Quat. Sci. Rev. 185, 122–134.
Taviani, M., 2014. Unpersisting persististrombus: a Mediterranean story. Vieraea Folia Sci. Biol Canar 9–18.
Thompson, H., Curran, A., Wilson, M.A., White, B., 2011. Sea-level oscillations during the last interglacial highstand recorded by Bahamas corals. Nat. Geosci. 4, 684–687.
Trenhaile, A.S., 2015. Coastal notches: their morphology, formation, and function. Earth-Sci. Rev. 150, 285–304.
Vacchi, M., Ermolli, E.R., Morhange, C., Ruello, M.R., Di Donato, V., Di Vito, M.A., Boetto, G., 2020. Millennial variability of rates of sea-level rise in the ancient harbour of Naples (Italy, western Mediterranean Sea). Quatern. Res. 93, 284–298.
Zanchetta, G., Bini, M., Isola, I., Pappalardo, M., Ribolini, A., Consoloni, I., Boretto, G., Fucks, E., Ragaini, L., Terrasi, F., 2014. Middle-to late-Holocene relative sea-level changes at Puerto Deseado (Patagonia, Argentina). The Holocene 24, 307–317.
Zanchetta, G., Giaccio, B., Bini, M., Sarti, L., 2018. Tephrostratigraphy of Grotta del Cavallo, Southern Italy: insights on the chronology of Middle to Upper Palaeolithic transition in the Mediterranean. Quat. Sci. Rev. 182, 65–77.